Development of two-dimensional groundwater flow simulation model using meshless method based on MLS approximation function in unconfined aquifer in transient state

Ali Mohtashami, Abolfazl Akbarpour and Mahdi Mollazadeh

ABSTRACT

In recent decades, due to reduction in precipitation, groundwater resource management has become one of the most important issues considered to prevent loss of water. Many solutions are concerned with the investigation of groundwater flow behavior. In this regard, development of meshless methods for solving the groundwater flow system equations in both complex and simple aquifers' geometry make them useful tools for such investigations. The independency of these methods to meshing and remeshing, as well as its capability in both reducing the computation requirement and presenting accurate results, make them receive more attention than other numerical methods. In this study, meshless local Petrov–Galerkin (MLPG) is used to simulate groundwater flow in Birjand unconfined aquifer located in Iran in a transient state for 1 year with a monthly time step. Moving least squares and cubic spline are employed as approximation and weight functions respectively and the simulated head from MLPG is compared to the observation results and finite difference solutions. The results clearly reveal the capability and accuracy of MLPG in groundwater simulation as the acquired root mean square error is 0.757. Also, with using this method there is no need to change the geometry of aquifer in order to construct shape function.

Key words | Birjand unconfined aquifer, groundwater flow, meshless local Petrov–Galerkin, transient state

Ali Mohtashami
Abolfazl Akbarpour (corresponding author)
Mahdi Mollazadeh
Department of Civil Engineering,
University of Birjand,
Birjand,
Iran
E-mail: *akbarpour@birjand.ac.ir*

INTRODUCTION

Understanding groundwater flow behavior is of high importance among hydrogeologists. They have tried to investigate the aquifer behavior in all aspects due to the low amount of precipitation in many places in the world. The way to recognize this action is to study the related governing equations. Therefore simulation of groundwater flow system, especially in arid zones is essential for the government and water scientists because of increasing rates of demand on groundwater reservoirs (Sadeghi Tabas *et al.* 2016).

Technically, the governed equations of groundwater flow can be solved by some numerical methods such as finite difference method (FDM) and finite element method (FEM). These methods are mesh based and in addition to their benefits they have some drawbacks related to the meshes. Many scientists have tried to resolve these shortages but FDM and FEM have their problems in the field of meshing. Using rectangular meshes makes the FDM amongst the most simple method for programming. However, it has its own limitations as meshes may not cover the whole domain precisely. Moreover, some problems concerned with changeable boundaries and constant update of the domain geometry is a time-consuming and complex task.

doi: 10.2166/hydro.2017.024

In order to address such problems, a newly numerical method, called the meshless method, has been developed. The meshless method is a numerical technique to solve problems simply. This method is used to change partial differential equations into a system of equations for the entire domain without the use of a mesh (Mategaonkar & Eldho 2011). Recently, there has been great attention focused on the development of 'meshless methods' to reduce meshing problems (Li *et al.* 2003). The first idea of meshless methods was introduced by Gingold & Monaghan (1977). They used smoothed particle hydrodynamics for modeling specified phenomena. The main idea of these methods is to approximate a function in the entire domain by just using scattered nodes. Atluri & Zhu (1998) presented a new meshless method called meshless local Petrov–Galerkin (MLPG). They developed local symmetric weak form to solve Laplace and Poisson equations and found this method capable and accurate (Atluri & Zhu 1998).

There has been little research into groundwater flow modeling using meshless methods. Mategaonkar & Eldho (2011) used a meshless method based on point collocation called polynomial point collocation method for the groundwater flow simulation in unconfined aquifers (Mategaonkar & Eldho 2011). Their case study regions include two presumptive aquifers in one- and two-dimensional and one real aquifer. Their results in hypothetical aquifers were compared with the FEM and analytical solutions. Kovarik & Muzik (2013) used a combination of two numerical methods, radial basis function (RBF) and the local boundary integral element method, to solve the unsteady density-driven groundwater flow in a rectangular case study (Kovarik & Muzik 2013). Swathi & Eldho (2013) simulated groundwater flow in a two-dimensional (2D) presumptive rectangular confined aquifer with MLPG with Gaussian RBF. They found their used method effective (Swathi & Eldho 2014). Swathi & Eldho (2014) also simulated groundwater flow in an unconfined aquifer with MLPG with Gaussian RBF as weight and shape functions. They chose both weight function and approximation function from one space. Also, to keep the size of all support domains equal they considered some dummy nodes in the aquifer (Swathi & Eldho 2014).

Recently, numerous studies have been related to the simulation of groundwater flow in the Birjand unconfined aquifer. Sadeghi Tabas *et al.* (2016) presented research that linked multi-algorithm genetically adaptive search method with a groundwater model to define pumping rates within a well-distributed set of Pareto solutions (Sadeghi Tabas *et al.* 2016). Hamraz *et al.* (2015) assessed parameter uncertainty of groundwater simulation in the Birjand aquifer. They modeled Birjand aquifer in Matlab using MODFLOW. They evaluated parameter uncertainty using GLUE (generalized likelihood uncertainty estimation). Their results showed that the performance of the GLUE was satisfactory (Hamraz *et al.* 2015). Ghoochanian *et al.* (2013) developed a model that linked MODFLOW and WEAP to manage water resources in the Birjand aquifer.

In this paper, the MLPG method is employed to solve the time-dependent groundwater flow equation in Birjand unconfined aquifer located in the east of Iran. The shape and weight functions are chosen from two different spaces. The weight function is cubic spline, moreover, a moving least squares (MLS) approximation function has been chosen as interpolation function. Finally, the simulated head is compared with the observation results and FDM (MODFLOW) solutions for each time step.

METHODS

Geographical location of the case study

The Birjand unconfined aquifer is located in South Khorasan province in the east of Iran. The area of this aquifer is almost 265 km^2. Mean annual precipitation in Birjand plain is 160 mm and generally this region is placed in an arid zone. The slope is shallow in the west part of the plain. The groundwater system is one-layer unconfined aquifer with changeable thickness of 5–225 m. (Sadeghi Tabas *et al.* 2016). Figure 1 shows the geographical location of the Birjand aquifer in Iran.

MLS method

MLS approximations were firstly introduced in the field of computational solid mechanics by means of the diffuse element method by Nayroles *et al.* (1992). Since then, this function has been utilized in the element-free Galerkin method by Belytschko *et al.* (1994). Now, it is an alternative

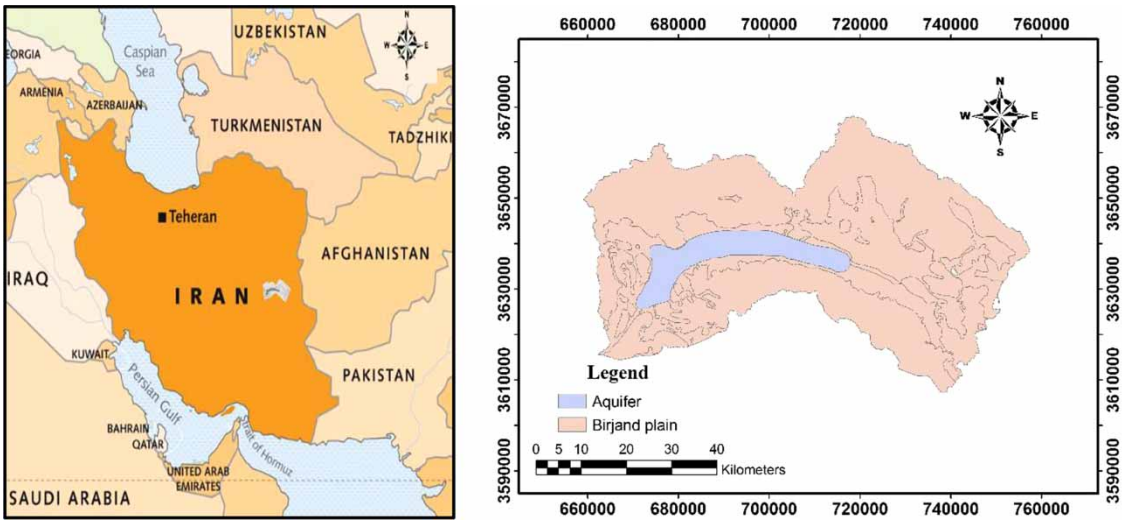

Figure 1 | Geographical location of Birjand aquifer.

approach for constructing meshless shape functions for approximation (Liu & Gu 2005). Due to two important characteristics, much attention has been attracted toward the MLS approximation: (1) the approximated field function is continuous and smooth in the whole problem domain when adequate nodes are used; and (2) it is able to produce an approximation with the desired order of consistency (Liu 2002).

The hydraulic head (U_I) of groundwater in an aquifer is needed to compute. The MLS approximation of hydraulic head $(U^h(X))$ can be defined as (Park & Leap 2000):

$$U^h(X) = \sum_j^m p_j(X)a_j(X) = P^T(X)a(X). \quad (1)$$

m is the number of the basis function $P(X)$ and $a(X)$ is a vector of unknown coefficient given by:

$$a^T(X) = \{a_1(X)\ a_2(X)\ \ldots\ a_m(X)\}. \quad (2)$$

In Equation (1), the basis function $P(X)$ is built using monomials from the Khayyam–Pascal triangle. In one-dimensional space, a complete polynomial basis of order l is given by:

$$P^T(X) = \left\{1\ x\ x^2\ \ldots\ x^l\right\}. \quad (3)$$

and in 2D space:

$$P^T(X, Y) = \left\{1\ x\ y\ x^2\ xy\ y^2 \ldots\ y^l\right\}. \quad (4)$$

In this study, the quadratic basis $p^T(x) = \{1\ \ x\ \ y\ \ x^2\ \ xy\ \ y^2\}$ is used.

The functional J must be minimized with respect to $a(X)$:

$$J = \sum_I^n W(X - X_I)\left[U^h(X) - U_I\right]^2. \quad (5)$$

where U_i are the nodal unknowns associated with the neighbors nodes X_i of point x and $W(X - X_I)$ is a weight function of ith node whose value decreases as the distance between X and X_i increases (Liu 2002).

The minimization condition for Equation (5) requires:

$$\frac{\partial J}{\partial a} = 0. \quad (6)$$

which leads to the linear equation system:

$$a(X)A(X) = B(X)U_s. \quad (7)$$

Assuming that the MLS moment matrix A is invertible, Equation (7) can then be solved for $a(x)$:

$$a(X) = A^{-1}(X)B(X)U_s. \quad (8)$$

$A(X)$, $B(X)$ and U_s are computed:

$$A(X) = \sum_I^n W(X_I)p(X_I)P^T(X_I). \quad (9)$$

$$B(X) = [W_1 p(x_1)\ W_2 p(x_2)\ \ldots\ W_n p(x_n)]. \quad (10)$$

$$U_s = [U_1\ U_2\ \ldots\ U_n]. \quad (11)$$

Substituting Equation (9) back into Equation (1):

$$U^h(X) = \sum_I^n \sum_j^m P_j(X)\left(A^{-1}(X)B(X)\right)_{jI} U_I. \quad (12)$$

In the simpler form:

$$U^h(X) = \sum_I^n \phi_I(X) U_I. \quad (13)$$

where $\varnothing(X)$ is the matrix of MLS shape function.

Choice of the weight function

Choosing the weight function plays a significant role in the efficiency of the MLS approximation function (Liu & Gu 2005). The choice of $W_i(X)$ is made. It has the following features: it is only strictly positive in a subdomain Ω_s containing X_i, but is zero outside this domain. Ω_s is called the support of the function $W_i(X)$ or the domain of influence of the node X_i. $W_i(X)$ reduces with the distance between X_i and X. Several weight functions can be used. In this study, the cubic spline weight function is used:

$$W_i(X) = \begin{cases} \frac{2}{3} - 4\overline{r_i^2} + 4\overline{r_i^3} & \overline{r_i} \le 0.5 \\ \frac{4}{3} - 4\overline{r_i} + 4\overline{r_i^2} - \frac{4}{3}\overline{r_i^3} & 0.5 < \overline{r_i} \le 1 \\ 0 & \overline{r_i} > 1 \end{cases} \quad (14)$$

In this equation $\overline{r_i} = \frac{d_i}{r_w} = \frac{|x - x_i|}{r_w}$ and r_w is the influence radius of node x_i. For each node, r_w must be selected in a way that the number of non-zero weight functions be more than each term in the polynomial.

MLPG method

This method is a truly meshless method, as it does not need a 'mesh', either for purposes of interpolation of the solution variables, or for the integration stage (Atluri & Zhu 2000). This method employs a local weak form to solve the equations. MLS approximation function is utilized for approximating. MLPG was first introduced by Atluri & Zhu (1998).

Discretization of groundwater flow equation in unconfined aquifer with MLPG method

The governing equation in groundwater flow modeling in unconfined aquifer is:

$$\frac{\partial}{\partial x}\left(k_x \frac{\partial H}{\partial x}\right) + \frac{\partial}{\partial y}\left(k_y \frac{\partial H}{\partial y}\right) + \frac{\partial}{\partial z}\left(k_z \frac{\partial H}{\partial z}\right) = \frac{S_s \partial H}{\partial t} \pm R. \quad (15)$$

where k_x, k_y and k_z indicate the hydraulic conductivity coefficients (L/T). H, S_s and R show the pressure head (L), specific storage (1/L) and recharge or discharge rate per unit volume (1/T) (positive or negative) respectively. In the unconfined aquifer, the thickness of saturated layer varies by groundwater table. Some assumptions proposed by Dupuit (1863) are:

(a) the flow is horizontal;
(b) the hydraulic gradient is equal to slope of the free surface.

The equation is based on the Dupuit (1863) assumption and continuity equation as follows:

$$\frac{\partial}{\partial x}\left(k_x H \frac{\partial H}{\partial x}\right) + \frac{\partial}{\partial y}\left(k_y H \frac{\partial H}{\partial y}\right) = \frac{S_y \partial H}{\partial t} + R. \quad (16)$$

where S_y is specific yield.

Since:

$$\frac{\partial H^2}{\partial x} = 2H\frac{\partial H}{\partial x} \text{ and } \frac{\partial H^2}{\partial y} = 2H\frac{\partial H}{\partial y} \quad (17)$$

with substitution of Equation (17) in Equation (16):

$$\frac{\partial}{\partial x}\left(k_x \frac{\partial H^2}{\partial x}\right) + \frac{\partial}{\partial y}\left(k_y \frac{\partial H^2}{\partial y}\right) = 2 \times \left(\frac{S_y \partial H}{\partial t} + R\right). \quad (18)$$

Since Birjand unconfined aquifer is isotropic:

$$k\left[\left(\frac{\partial^2 H^2}{\partial x^2}\right)+\left(\frac{\partial^2 H^2}{\partial y^2}\right)\right]=2\times\left(\frac{S_y\partial H}{\partial t}+R\right). \tag{19}$$

with using weighted residual method:

$$\iint_\Omega W_i k\left(\frac{\partial^2 H^2}{\partial x^2}+\frac{\partial^2 H^2}{\partial y^2}\right)d\Omega=2\iint_\Omega W_i\left(\frac{S_y\partial H}{\partial t}+R\right)d\Omega. \tag{20}$$

$$\iint_\Omega W_i k\left(\frac{\partial^2 H^2}{\partial x^2}\right)d\Omega+\iint_\Omega W_i k\left(\frac{\partial^2 H^2}{\partial y^2}\right)d\Omega =2\iint_\Omega W_i\frac{S_y\partial H}{\partial t}d\Omega+2\iint_\Omega W_i R d\Omega. \tag{21}$$

By using integration of parts in Equation (21):

$$k\left[\int_\Gamma W_i\frac{\partial H^2}{\partial x}d\Gamma-\iint_\Omega\frac{\partial W_i}{\partial x}\frac{\partial H^2}{\partial x}d\Omega+\int_\Gamma W_i\frac{\partial H^2}{\partial y}d\Gamma-\iint_\Omega\frac{\partial W_i}{\partial y}\frac{\partial H^2}{\partial y}d\Omega\right] =2\iint_\Omega W_i\frac{S_y\partial H}{\partial t}d\Omega+2\iint_\Omega W_i R d\Omega. \tag{22}$$

Since the Birjand aquifer has no normal flow over its boundary, the first and third term in the left side of Equation (22) vanish:

$$-k\left[\iint_\Omega\frac{\partial W_i}{\partial x}\frac{\partial H^2}{\partial x}d\Omega+\iint_\Omega\frac{\partial W_i}{\partial y}\frac{\partial H^2}{\partial y}d\Omega\right] =2\iint_\Omega W_i\frac{S_y\partial H}{\partial t}d\Omega+2\iint_\Omega W_i R d\Omega. \tag{23}$$

Substituting Equation (17) in Equation (23):

$$-2k\left[\iint_\Omega\frac{\partial W_i}{\partial x}H\frac{\partial H}{\partial x}d\Omega+\iint_\Omega\frac{\partial W_i}{\partial y}H\frac{\partial H}{\partial y}d\Omega\right] =2\iint_\Omega W_i\frac{S_y\partial H}{\partial t}d\Omega+2\iint_\Omega W_i R d\Omega. \tag{24}$$

The approximate value for head is:

$$H=\sum_{i=1}^{m}H_i(t)\times\varnothing_i(x,y). \tag{25}$$

Substituting Equation (25) in Equation (24):

$$-2k\left[\iint_\Omega\frac{\partial W_i}{\partial x}H\times H\frac{\partial\varnothing}{\partial x}d\Omega+\iint_\Omega\frac{\partial W_i}{\partial y}H\times H\frac{\partial\varnothing}{\partial y}d\Omega\right] =2\iint_\Omega W_i\frac{S_y\partial H}{\partial t}d\Omega+2\iint_\Omega W_i R d\Omega. \tag{26}$$

In this study, the FDM in time is used. Forward finite difference approximation is employed for computation of the time derivative:

$$\frac{\partial H}{\partial t}=\frac{H^{n+1}-H^n}{\Delta t}. \tag{27}$$

Substituting Equation (27) in Equation (26):

$$-2k\left[\iint_\Omega\frac{\partial W_i}{\partial x}H^{n+1}\times H^n\frac{\partial\varnothing}{\partial x}d\Omega+\iint_\Omega\frac{\partial W_i}{\partial y}H^{n+1}\times H^n\frac{\partial\varnothing}{\partial y}d\Omega\right] =2\iint_\Omega W_i S_y\left(\frac{H^{n+1}-H^n}{\Delta t}\right)d\Omega+2\iint_\Omega W_i R d\Omega. \tag{28}$$

$$-2k\left[\iint_\Omega\frac{\partial W_i}{\partial x}H^n\frac{\partial\varnothing}{\partial x}d\Omega+\iint_\Omega\frac{\partial W_i}{\partial y}H^n\frac{\partial\varnothing}{\partial y}d\Omega\right] -2\iint_\Omega W_i S_y\left(\frac{1}{\Delta t}\right)d\Omega\times H^{n+1} =-2\iint_\Omega W_i S_y\left(\frac{H^n}{\Delta t}\right)d\Omega+2\iint_\Omega W_i R d\Omega. \tag{29}$$

This equation is similar to the linear equation:

$$[K]=-2k\left[\iint_\Omega\frac{\partial W_i}{\partial x}H^n\frac{\partial\varnothing}{\partial x}d\Omega+\iint_\Omega\frac{\partial W_i}{\partial y}H^n\frac{\partial\varnothing}{\partial y}d\Omega\right] -2\iint_\Omega W_i S_y\left(\frac{1}{\Delta t}\right)d\Omega. \tag{30}$$

$$[U] = H^{n+1}. \tag{31}$$

$$[F] = -2\iint_{\Omega} W_i S_y \left(\frac{H^n}{\Delta t}\right) d\Omega + 2\iint_{\Omega} W_i R d\Omega. \tag{32}$$

Equation (32) represents force body matrix. It indicates the rate of recharge or discharge of the aquifer. In other words, this matrix shows the interaction or extraction flow rate in two concentrated and distributed conditions.

The principles of groundwater modeling

Birjand aquifer was represented by using sets of nodes which were scattered uniformly in it. The word uniform means that the distance between two adjacent points in horizontal and vertical direction is 500 meters ($\Delta \boldsymbol{x} = \Delta \boldsymbol{y} = 500$ m). Input data, such as extraction wells, recharge and discharge rates, boundary conditions, hydraulic conductivity coefficient and specific yield of each node, were entered into the model. The algorithm of simulating with MLPG is presented in Figure 2.

The scattered nodal points in the domain are presented in Figure 3. Each blue point in the domain has four values: hydraulic head that should be computed, hydraulic conductivity coefficient, specific yield and the rate of recharge or discharge (please refer to the online version of this paper to see Figure 3 in color: http://dx.doi.org/10.2166/hydro.2017.024).

Boundary conditions

Generally, there are two classifications for boundary conditions in modeling of groundwater flow. One is nodes with a specified head (Dirichlet) boundary condition, and the other one is nodes with no flow or inactive (Neuman) boundary condition. Inactive nodes or no flow nodes are those for which no flow into or out of the nodes is permitted. Constant head nodes are those for which the head is specified in advance, and is held at this specified value through all time steps of the simulation. In the Birjand aquifer, there are 10 areas that have specified head boundary condition, nine inflow pathways and one outflow pathway. Figure 4 specifies these areas. The other boundary nodes have no flow boundary conditions, in other words they are defined as inactive nodes.

Wells

There are 190 extraction wells in the studied region. These pumping wells consist of 139 agricultural, 31 drinking water and 20 industrial wells. In this aquifer 10 observation wells were used to investigate the level of water table. Figures 5 and 6 show the location of extraction and observation wells with square and circle symbol respectively.

Recharge and discharge rate

Since the studied area is categorized as an arid region with low amounts of precipitation, this low precipitation is considered as the recharge value. This aquifer had 0.000727 m/day rain between 2011 and 2012 based on rain gauges employed in Birjand plain.

The volume of extracted water from extraction wells is used as the discharge rate in our proposed model.

Hydraulic conductivity coefficient and specific yield

In order to allocate hydraulic conductivity coefficient and specific yield in each node, the aquifer has been divided into polygons. This is done by ArcGIS software. For each polygon there is one value that represents the magnitude of the hydraulic conductivity coefficient and specific yield. All the nodes in each polygon have the same value as the polygon. The unit of hydraulic conductivity coefficient is m/day. Figures 7 and 8 indicate a divided aquifer for presenting hydraulic conductivity coefficient and specific yield parameters. These parameters are obtained from the results of pumping tests.

According to Figure 8, Birjand unconfined aquifer is divided into 48 polygons. Each polygon has a number as a legend. The value of the specific yield parameter for a polygon can be obtained based on its legend number from Table 1.

MODFLOW model

The groundwater flow equation is solved by a finite difference scheme using a groundwater modeling system (GMS). MODFLOW is a three-dimensional finite-difference groundwater model and engages certain equations for

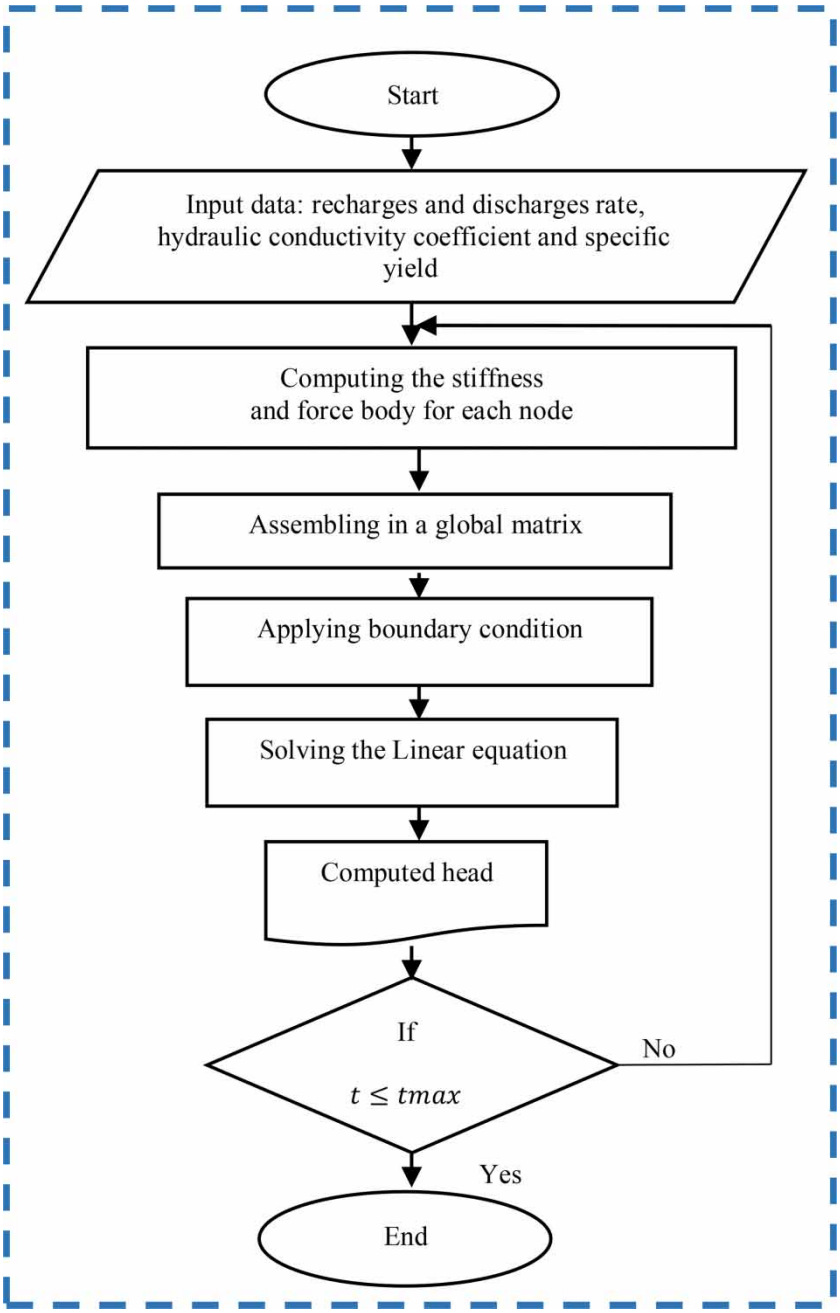

Figure 2 | Flowchart of groundwater flow modeling.

computing the head of groundwater in different cells of the aquifer. The model was first released in 1984 by the United States Geological Survey (USGS). Now, it is used as a popular package for simulation of groundwater flow in both steady and unsteady states. Modeling groundwater flow with a MODFLOW package requires accurate data from the aquifer.

The first step to simulate groundwater flow in GMS is to define a conceptual model. This is done to simplify the analysis of the field data in real conditions (Anderson

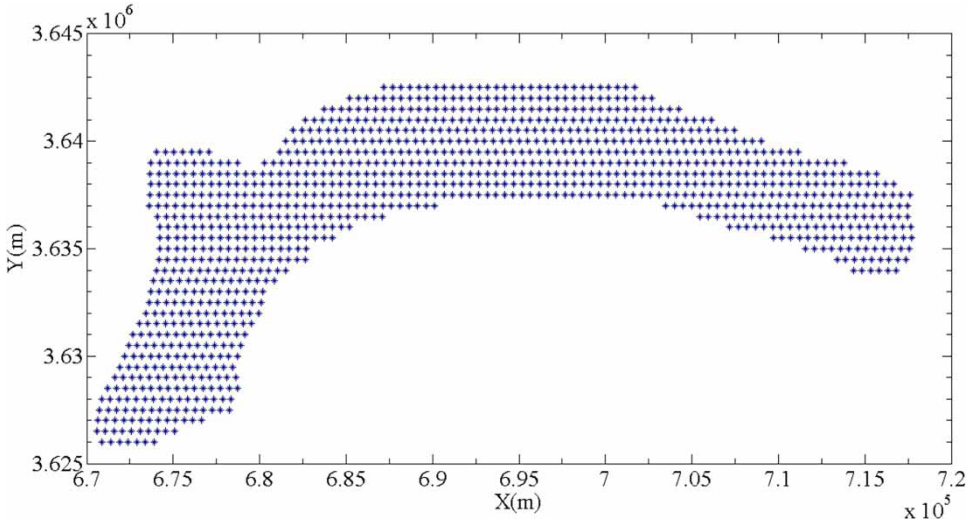

Figure 3 | Scattering nodal points in simulated aquifer in Matlab software.

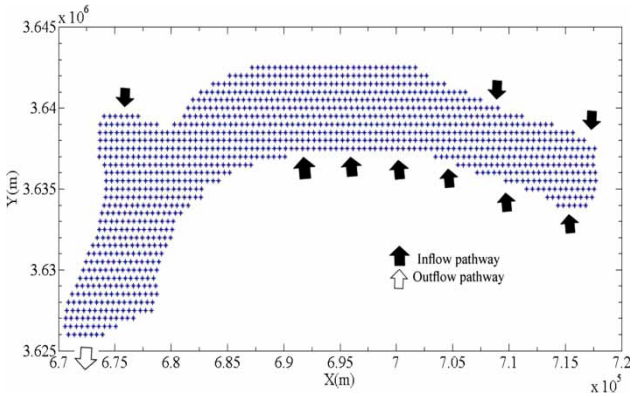

Figure 4 | Presented inflow and outflow pathways in Birjand aquifer.

& Woessner 1991). All the meteorological, hydrological and geophysics studies, geological investigation, well logs, water level fluctuation, type of groundwater flow system, and hydrodynamic coefficients are employed in the conceptual model. The conceptual model consists of definition of boundary, type and structure of aquifer and sources and sinks, etc. The next step is to choose an algorithm for solving the related equation. In the fourth stage the conceptual model is converted to a numerical model. This stage includes griding domain, definition of time steps and implied boundary conditions. Finally, the model is calibrated. Calibration means the

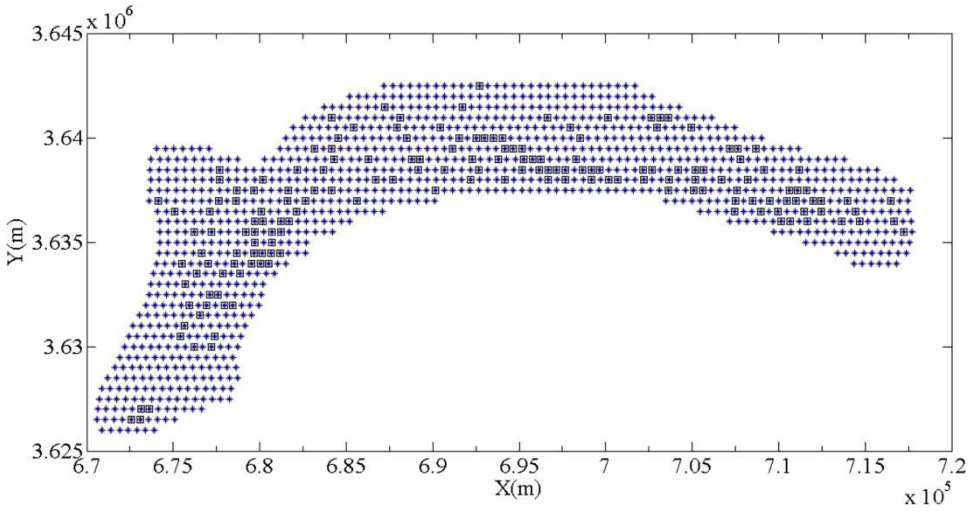

Figure 5 | Extraction wells in Birjand aquifer.

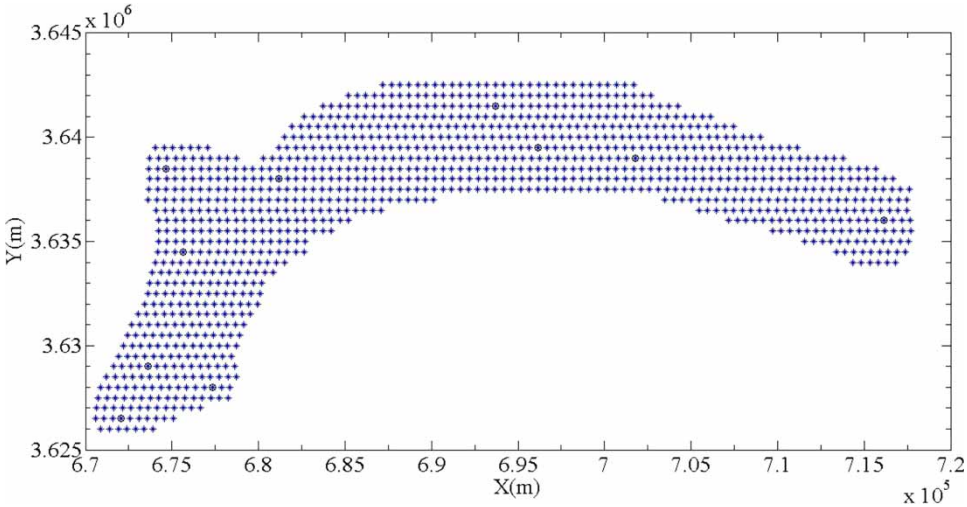

Figure 6 | The location of piezometers (observation wells) in the aquifer.

accommodation of simulation results with observation results.

Sadeghi Tabas *et al.* (2016) and Hamraz *et al.* (2015) modeled Birjand unconfined aquifer using the MODFLOW model. They developed their model based on available data, including well locations and measurements, geologic map, well logs, topography data, hydrography and recharge information.

Seven layers were used to construct the groundwater model. Aquifer boundary conditions, piezometers, pumping wells, surface recharge, drainage information, hydraulic conductivity and specific yield are applied to the MODFLOW model to create a groundwater numerical model (Sadeghi Tabas *et al.* 2016).

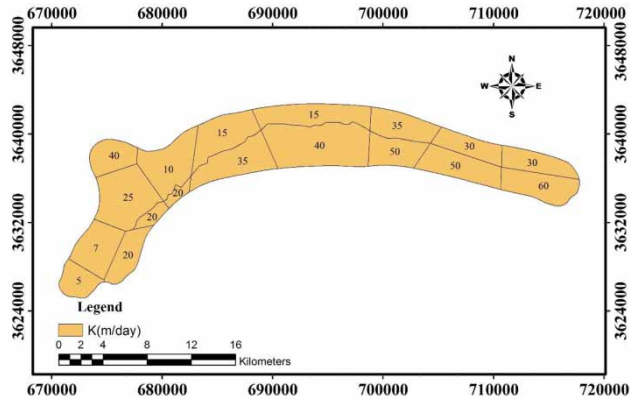

Figure 7 | Hydraulic conductivity polygons in Birjand aquifer.

RESULTS AND DISCUSSION

The groundwater flow in the Birjand unconfined aquifer is simulated with the MLPG and finite difference (MODFLOW) methods. The water level is computed for every node in each time step. To investigate the accuracy of the results, observed head in piezometers (observation wells) was compared with MLPG and FDM solutions. Figure 9 shows the comparison of these numerical methods and observed results for four random piezometers.

Tables 2 and 3 show the simulated head with using MLPG and FDM in comparison of observation data in each time step for two piezometers (piezometer 1 and 3).

Figures 9 and 10 show the change of hydraulic head along the aquifer in the first and last stress period (month) of 2010–2011.

The groundwater level has a maximum value of approximately 1,390 m in the east of the aquifer, and it decreases gradually while traveling to the west. The south-west has a minimum value around 1,264 m.

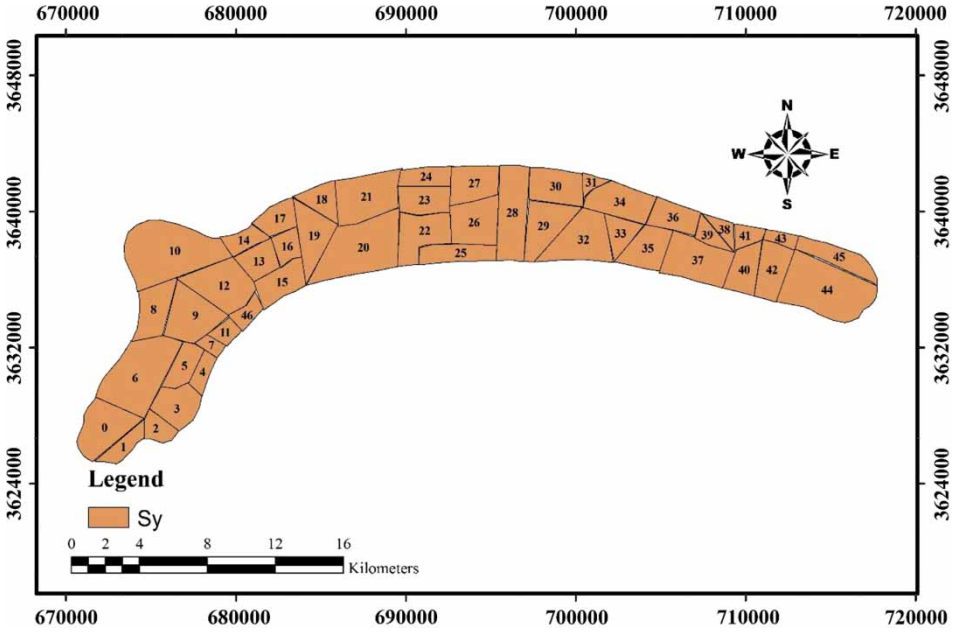

Figure 8 | Representation of specific yield polygons in Birjand aquifer.

Performance of the model

There are three criterion that were used to evaluate the error of the results. Mean error (ME), mean absolute error (MAE) and root mean square error (RMSE). Error estimation was computed using Equations (33)–(35) (Sadeghi Tabas *et al.* 2016):

$$ME = \frac{\sum_{j=1}^{m}\sum_{i=1}^{n}(h_o - h_s)}{m \times n} \tag{33}$$

$$MAE = \frac{\sum_{j=1}^{m}\sum_{i=1}^{n}|h_o - h_s|}{m \times n} \tag{34}$$

$$RMSE = \sqrt{\frac{\sum_{j=1}^{m}\sum_{i=1}^{n}(h_o - h_s)^2}{m \times n}} \tag{35}$$

where h_o, h_s indicates the observed and simulated heads respectively while 'm' is the number of monthly time steps and 'n' is the number of piezometers. These mentioned errors are computed in Table 4.

Actually, the allowable error associated with the field and model data should be under +1.9 m. In this study, the objective error is RMSE, according to Table 4 the RMSE of using MLPG and FDM methods are 0.757 and 1.197. They have significant differences. So the MLPG method reveals results with more accuracy than the FDM method.

Table 1 | Values of specific yield in polygons based on its number

Num	Specific yield	Num	Specific yield	Num	Specific yield
0	0.25	16	0.06	32	0.04
1	0.02	17	0.05	33	0.07
2	0.04	18	0.04	34	0.17
3	0.03	19	0.064	35	0.04
4	0.03	20	0.03	36	0.12
5	0.054	21	0.06	37	0.04
6	0.03	22	0.1	38	0.1
7	0.054	23	0.03	39	0.05
8	0.03	24	0.04	40	0.04
9	0.065	25	0.1	41	0.08
10	0.07	26	0.04	42	0.04
11	0.04	27	0.03	43	0.1
12	0.075	28	0.05	44	0.04
13	0.045	29	0.1	45	0.1
14	0.07	30	0.04	46	0.04
15	0.043	31	0.04	47	0.035

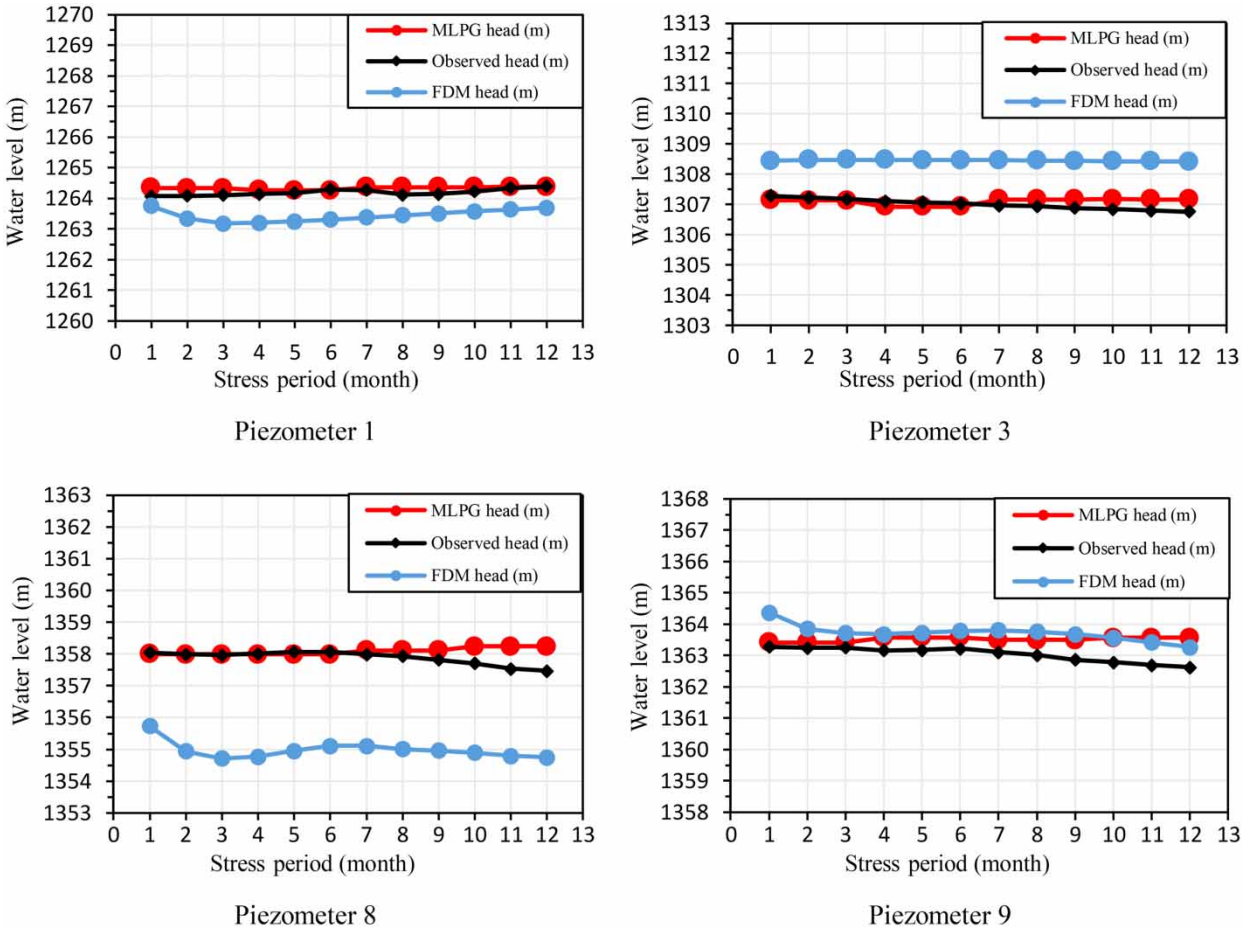

Figure 9 | Computed water level from MLPG, FDM in comparison with observed head.

Table 2 | Comparison in results of MLPG, FDM and observation in piezometer 1

Stress period (month)	MLPG head (m)	FDM head (m)	Observed head (m)
1	1,264.34	1,263.756	1,264.07
2	1,264.33	1,263.341	1,264.08
3	1,264.33	1,263.182	1,264.11
4	1,264.27	1,263.203	1,264.14
5	1,264.26	1,263.253	1,264.17
6	1,264.26	1,263.31	1,264.29
7	1,264.363	1,263.377	1,264.27
8	1,264.362	1,263.444	1,264.12
9	1,264.363	1,263.511	1,264.14
10	1,264.366	1,263.576	1,264.22
11	1,264.37	1,263.638	1,264.34
12	1,264.37	1,263.698	1,264.39

Table 3 | Comparison in results of MLPG, FDM and observation in piezometer 3

Stress period (month)	MLPG head (m)	FDM head (m)	Observed head (m)
1	1,307.145	1,308.44	1,307.29
2	1,307.134	1,308.474	1,307.23
3	1,307.134	1,308.479	1,307.18
4	1,306.927	1,308.476	1,307.11
5	1,306.928	1,308.473	1,307.07
6	1,306.928	1,308.471	1,307.04
7	1,307.168	1,308.466	1,306.97
8	1,307.166	1,308.458	1,306.94
9	1,307.166	1,308.448	1,306.89
10	1,307.176	1,308.437	1,306.85
11	1,307.175	1,308.427	1,306.8
12	1,307.175	1,308.418	1,306.77

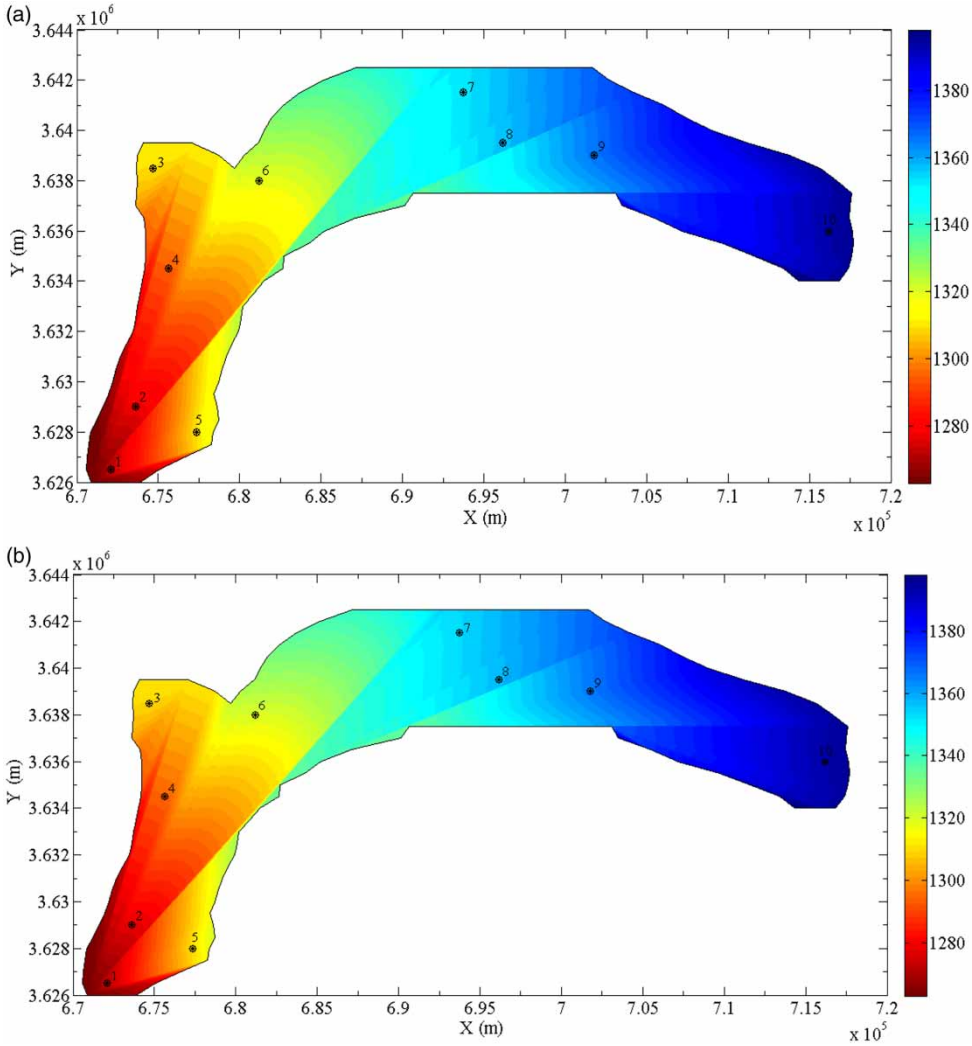

Figure 10 | The variability of hydraulic head in (a) the first stress period (b) the last stress period.

Table 4 | ME, MAE and RMSE errors

	MLPG method (m)	FDM method (MODFLOW) (m)
ME	–0.08	0.159
MAE	0.573	1.434
RMSE	0.757	1.197

CONCLUSIONS

In recent decades, reduction in precipitation, population growth and civilization developments caused an increase in underground water withdrawal and endangered the groundwater flow system balance. In this regard, water resources management has become one of the main issues under investigation for better resources management. The best way for managing water resources is to use a numerical method. In this study, Birjand unconfined aquifer with complex geometry located in east of Iran is modeled using MLPG. The shape and weight functions are chosen from two different spaces and cubic spline is employed as the weight function. Moreover, the MLS approximation function is used as the approximation function. The simulated head by MLPG was compared with the results of observation data and FDM (MODFLOW) solution. For four piezometers as an example, comparison among the solutions of these

methods was carried out. Also, the RMSE for MLPG solution was computed as 0.757. This value shows the high accuracy of the MLPG in simulating groundwater flow.

REFERENCES

Anderson, M. & Woessner, W. 1991 *Applied Groundwater Modeling Simulation of Flow and Advective Transport*, 1st edn. Academic Press, USA.

Atluri, S. N. & Zhu, T. L. 1998 A new meshless method (MLPG) approach in computational mechanics. *Comput. Mech.* **22** (2), 117–127.

Atluri, S. N. & Zhu, T. L. 2000 The meshless local Petrov–Galerkin (MLPG) approch for solving problems in elasto plastic. *Comput. Mech.* **25**, 169–179.

Belytschko, T., Lu, Y. Y. & Gu, L. 1994 Elements free Galerkin methods. *Int. J. Numer. Meth. Eng.* **30** (2), 229–256.

Dupuit, J. 1863 *Estudes Theoriques et Pratiques sur le Mouvement des Eaux*. Dunod, Paris.

Ghoochanian, E., Etebari, B. & Akbarpour, A. 2013 Integrating groundwater management with WEAP and MODFLOW models (case study: Birjand Plain, east of Iran). Modflow and More: Translating Science into Practice – IGWMC.

Gingold, R. A. & Monaghan, J. J. 1977 Smoothed particle hydrodynamics: theory and application to non-spherical stars. *Mon. Not. R. Astron. Soc.* **181** (3), 375–389.

Hamraz, B. S., Akbarpour, A., Pourreza Bilondi, M. & Sadeghi Tabas, S. 2015 On the assessment of ground water parameter uncertainty over an arid aquifer. *Arab. J. Geosci.* **8** (12), 10759–10773.

Kovarik, K. & Muzik, J. 2013 A meshless solution of two dimensional density-driven groundwater flow. *Eng. Anal. Bound. Elem.* **37**, 187–196.

Li, J., Chen, Y. & Pepper, D. 2003 Radial basis function method for 1-D and 2-D groundwater. *Comput. Mech.* **32** (1), 10–15.

Liu, G. 2002 *Mesh Free Methods: Moving Beyond the Finite Element Method*. CRC Press, Boca Raton.

Liu, G. R. & Gu, Y. T. 2005 *An Introduction to Meshfree Methods and Their Programming*. Springer, Singapore.

Mategaonkar, M. & Eldho,, T. I. 2011 Simulation of groundwater flow in unconfined aquifer using meshfree point collocation method. *Eng. Anal. Bound. Elem.* **35**, 700–707.

Nayroles, N., Touzot, G. & Villon, P. 1992 Generalizing the finite element method: diffuse approximation and diffuse elements. *Comput. Mech.* **10** (5), 307–318.

Park, Y. C. & Leap, D. I. 2000 Modeling groundwater flow with a free and moving boundary using the element-free Galerkin (EFG) method. *Geosci. J.* **4** (3), 243–249.

Sadeghi Tabas, S., Samadi, S. Z., Akbarpour, A. & Pourreza Bilondi, M. 2016 Sustainable groundwater modeling using single-and multi-objective optimization algorithms. *J. Hydroinform.* **19** (1), 97–114.

Swathi, B. & Eldho, T. I. 2013 Groundwater flow simulation in confined aquifers using meshless local Petrov-Galerkin (MLPG) method. *ISH Journal of Hydraulic Engineering* **19** (3), 335–348.

Swathi, B. & Eldho, T. I. 2014 Groundwater flow simulation in unconfined aquifers using meshless local Petrov-Galerkin method. *Eng. Anal. Bound. Elem.* **48**, 43–52.

First received 7 February 2017; accepted in revised form 21 March 2017. Available online 12 May 2017